Electronic Supplementary Information

Hierarchically structured Polymeric Ionic Liquids and Polyvinylpyrrolidone mat-fibers fabricated by electrospinning

Silvia Montolio,[a] Gabriel Abarca,[b] Raúl Porcar,[a] Jairton Dupont,[c] María Isabel Burguete,[a] Eduardo García-Verdugo,[*a] and Santiago V. Luis[*a c]

[a] *Universidad Jaume I, Departamento de Química Inorgánica y Orgánica, Campus del Riu Sec, E-12071 Castellón, Spain*
[b] *Laboratory of Molecular Catalysis, Institute of Chemistry – UFRGS, Avenida Bento Gonçalves, 9500, Porto Alegre 91501-970 RS Brazil*
[c] *School of Chemistry, University Park, Nottingham, NG7 2RD, UK*

Table of Contents

Electrospinning equipment

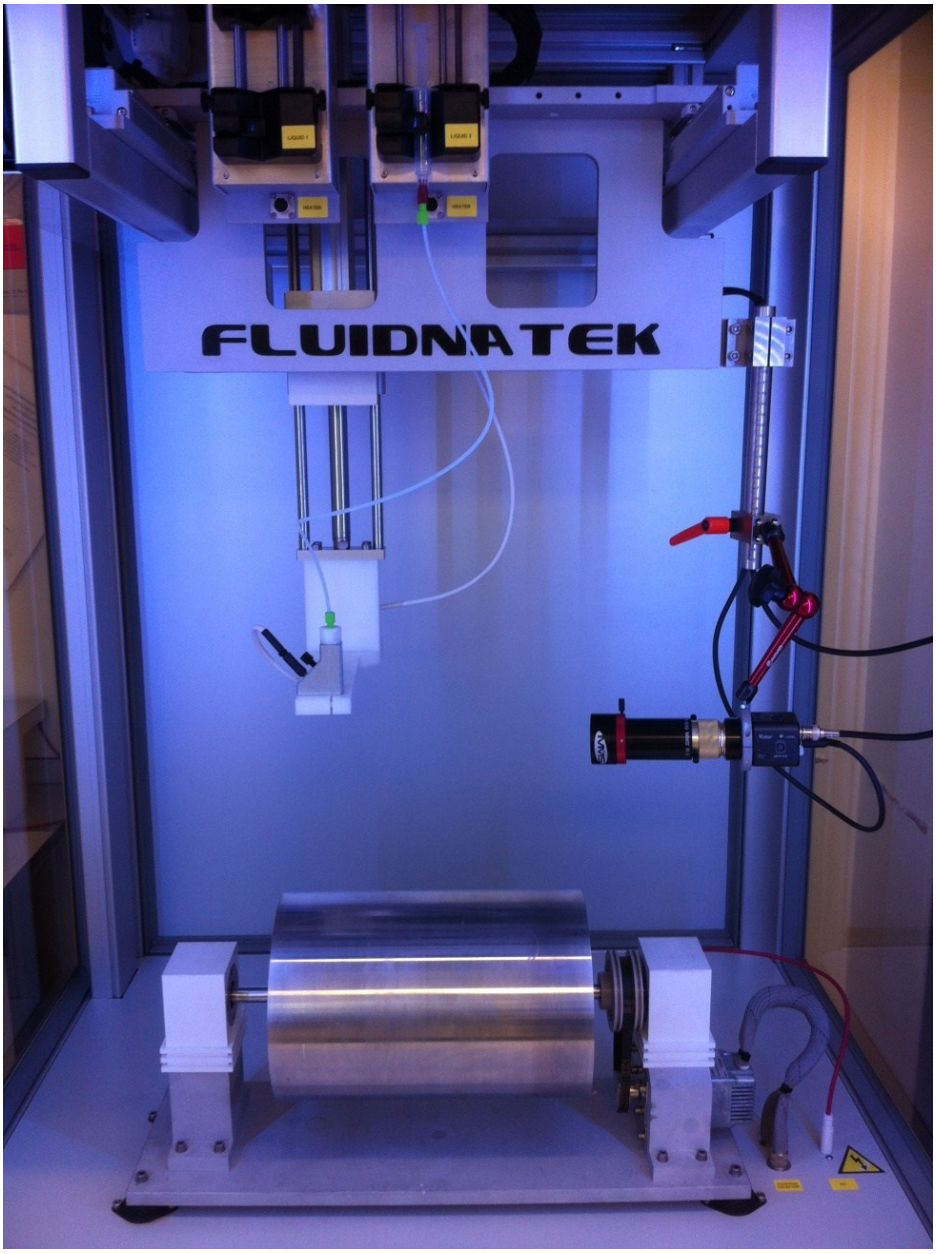

Figure S1. Image of the electrospinner Fluidnatek LE 100.V1, BioInicia.

Microscope and SEM images of films

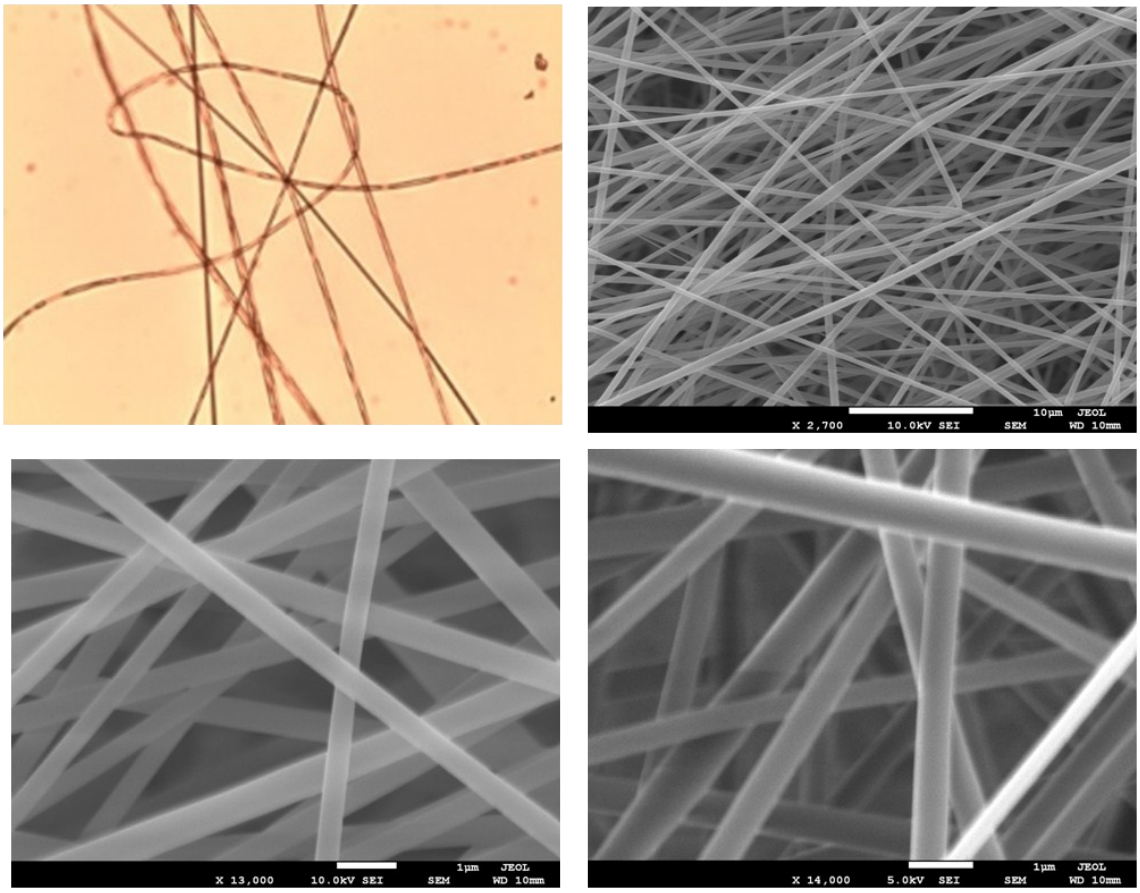

Figure S2. Microscope and SEM images for film **2/PVP.**

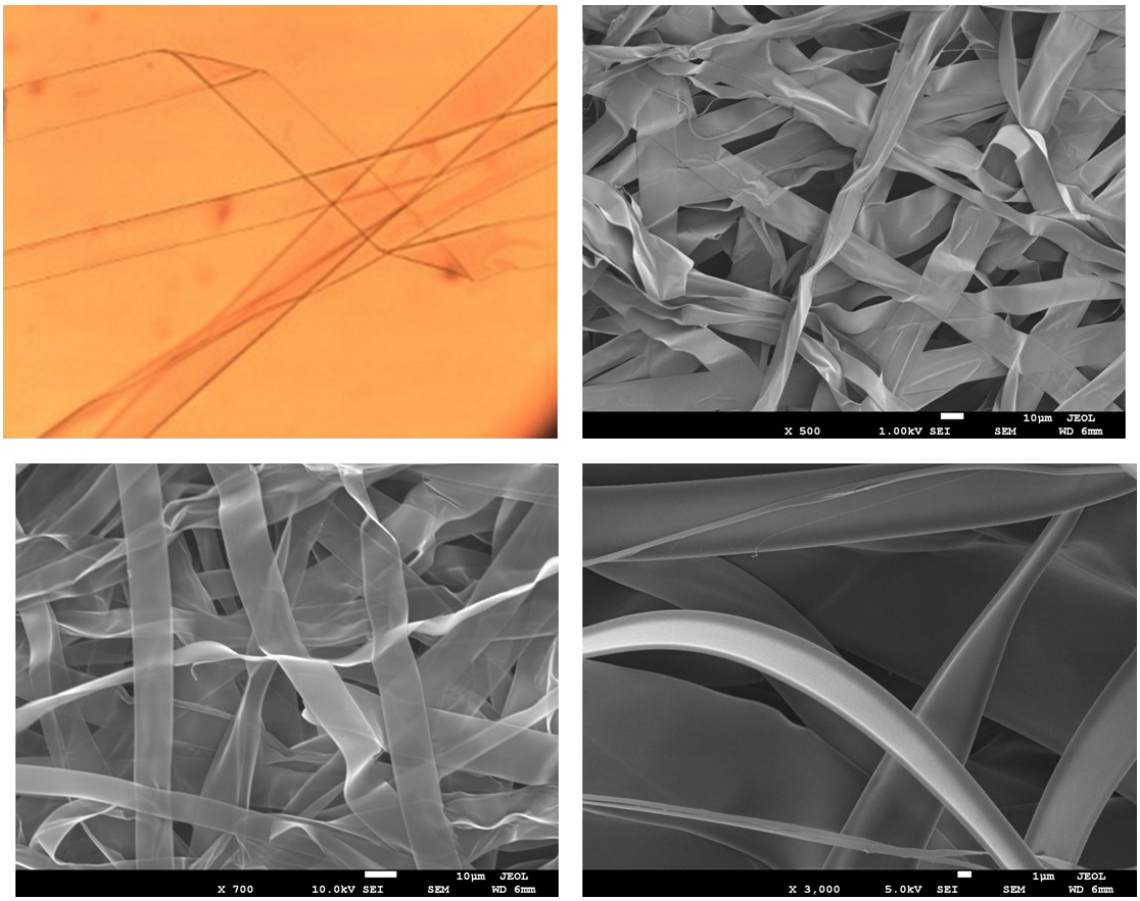

Figure S3. Microscope and SEM images for film **4a/PVP.**

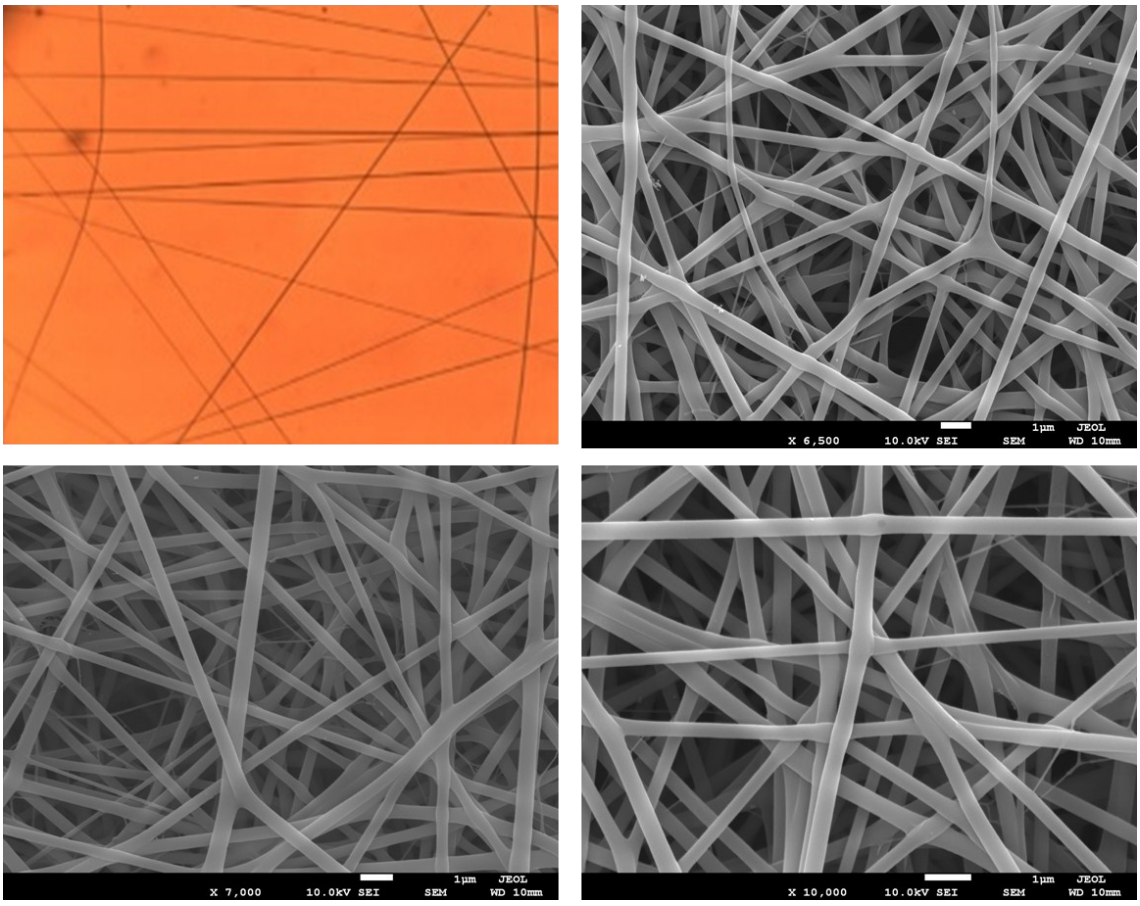

Figure S4. Microscope and SEM images for film **5a/PVP.**

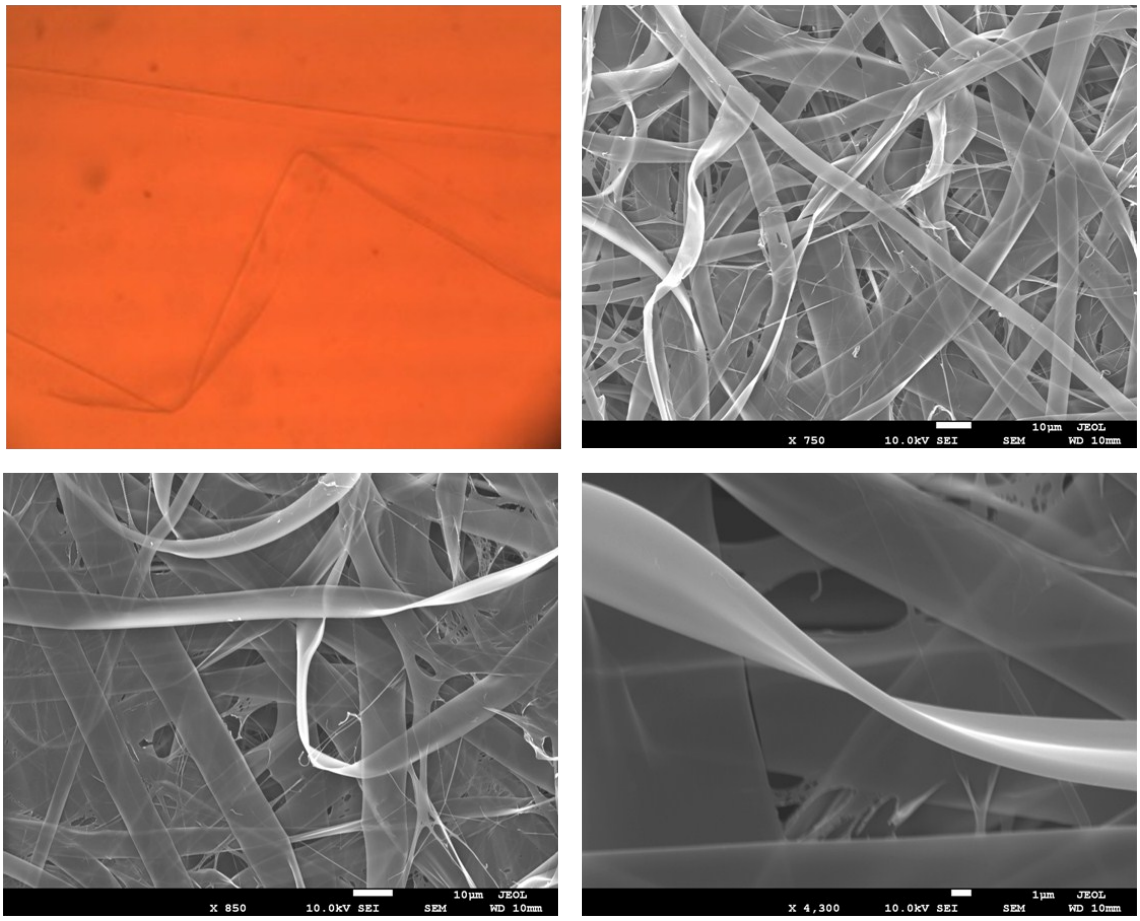

Figure S5. Microscope and SEM images for film **4b/PVP.**

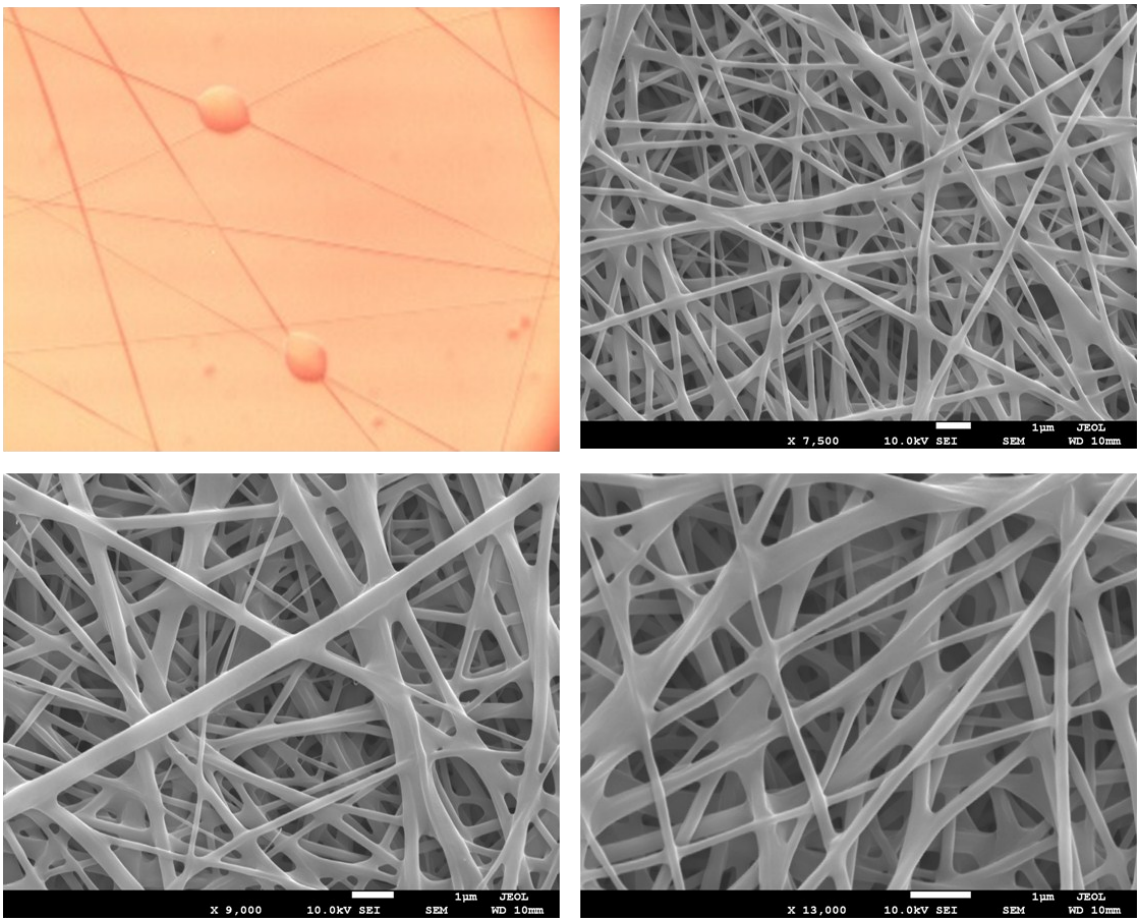

Figure S6. Microscope and SEM images for film **5b/PVP.**

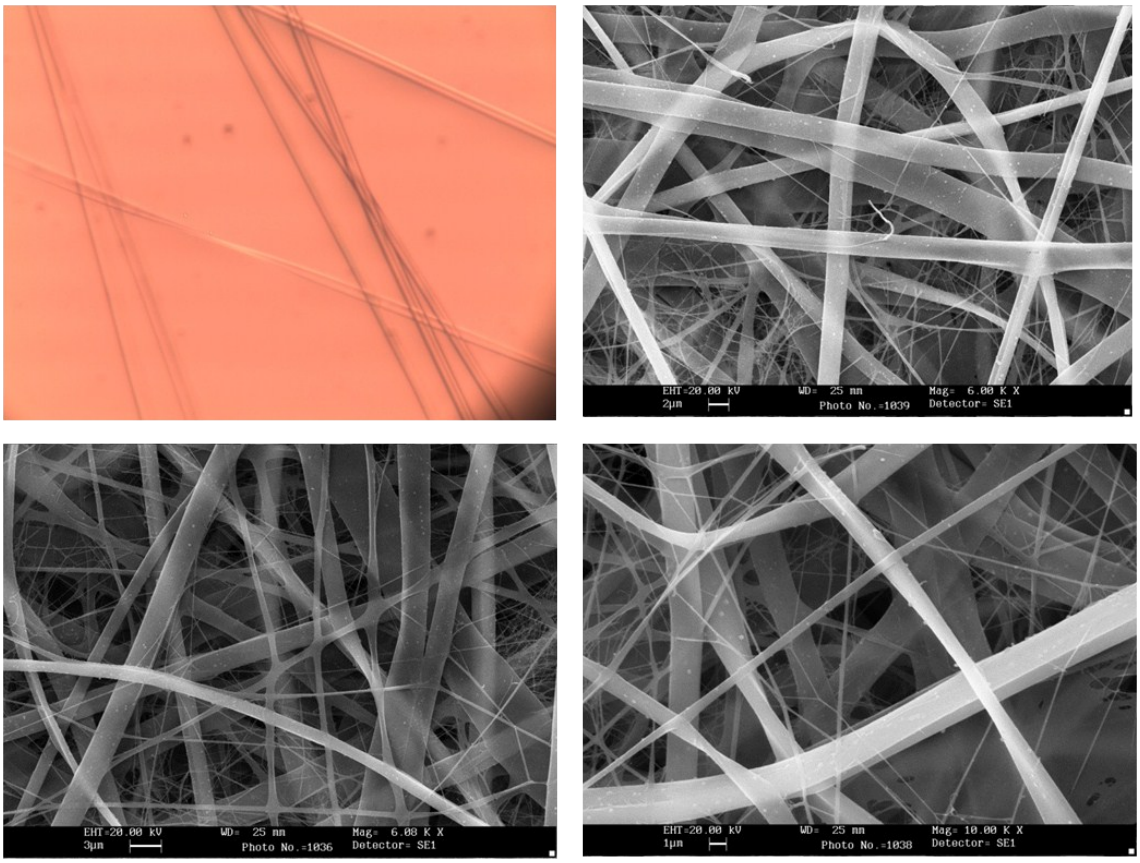

Figure S7. Microscope and SEM images for film **6a/PVP** (ribbons size 2.03 µm).

a)

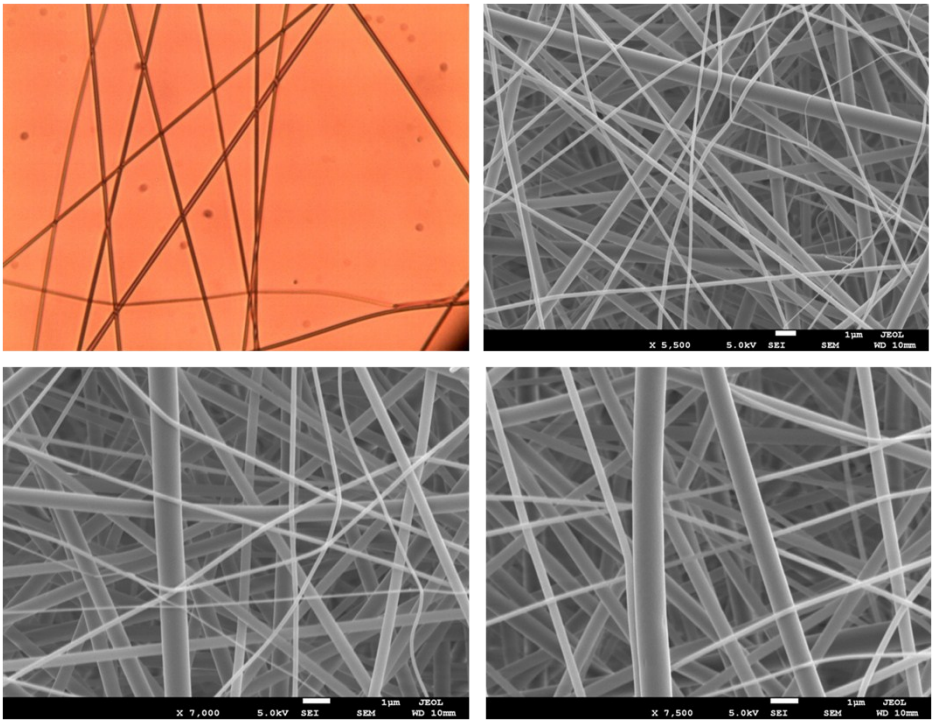

b)

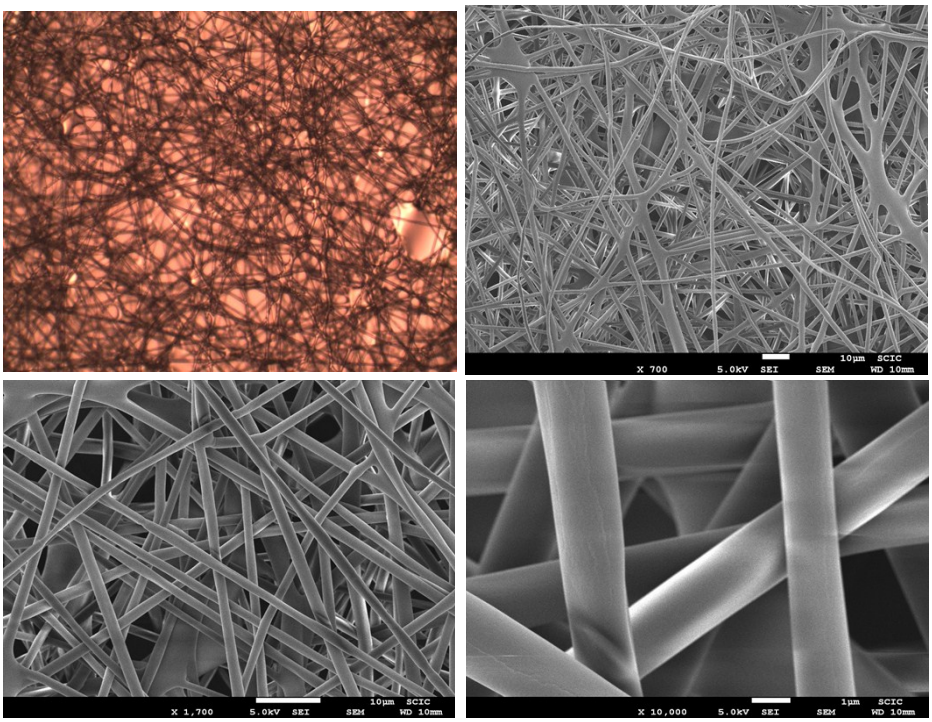

Figure S8. Microscope and SEM images for film **PVP.** a) electrospun from MeOH solution (fine fibers size 0.2 µm and big fibers size 0.6 µm). b**)** electrospun from DMF solution (fine fibers size 1.7 µm).

Viscosity results

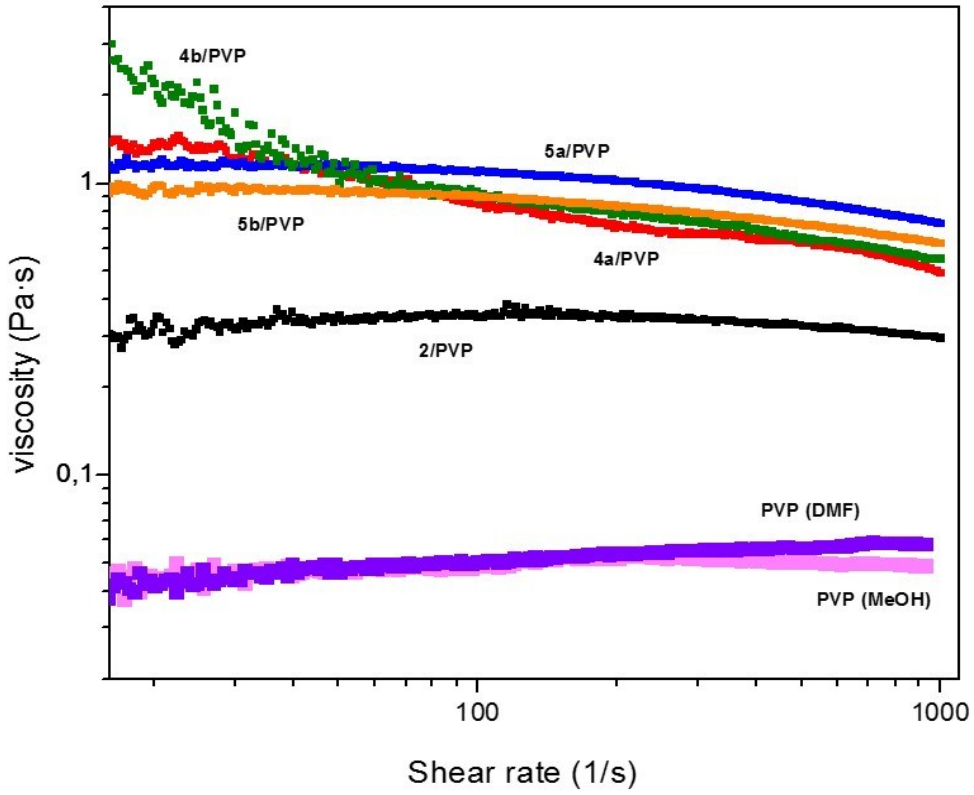

Figure S9. Viscosity obtained for the different polymeric mixtures showed in Table 1.

The behavior of the viscosity as a function of shear rate differs for the different mixtures as observed in Figure S9. Thus, the mixture formed by **2/PVP** shows a quasi-newtonian behavior, displaying a minimum change with the shear rate. A partly related curve is observed for **5a/PVP** and **5b/PVP** containing NTf_2^- as the counteranion. In this case, the viscosity values are always significantly higher than those of **2/PVP** and only display a minor decrease with shear rate. A very different pattern is detected, however, for **4a/PVP** and **4b/PVP** containing Cl^- as the counteranion. In this case, the viscosity detected at low shear rates is higher than the one measured for **5a/PVP** and **5b/PVP**, but experiment a sharp decrease with the initial increments in shear rate. This is particularly relevant for **4b/PVP** containing Cl^- as the counteranion and octyl as the N-substitution in the imidazolium fragment, revealing that both coulombic/hydrogen bonding and hydrophobic interactions contribute to this behavior. This suggests the presence of very strong interactions in the mixture through the combination of these two structural elements. This is confirmed when the viscosity of the PVP solutions in either MeOH or DMF was study. The values of viscosity are significantly lower at least one order of magnitude (< 0.005 Pa s) in comparison than those found for the different polymeric mixtures confirming the strong interaction between the polymers forming the mixture

TGA results

a)

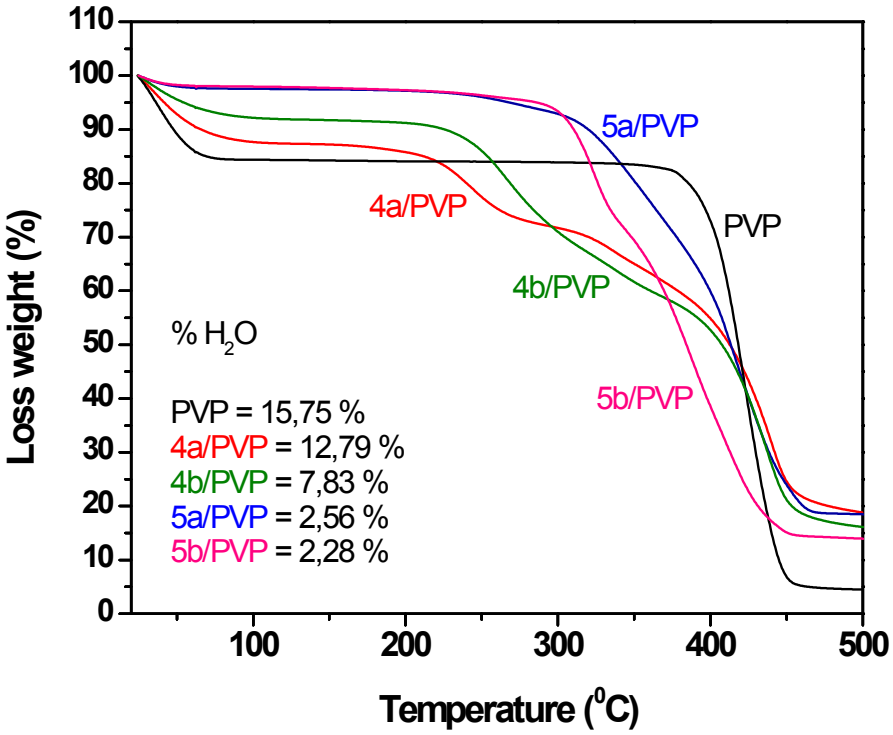

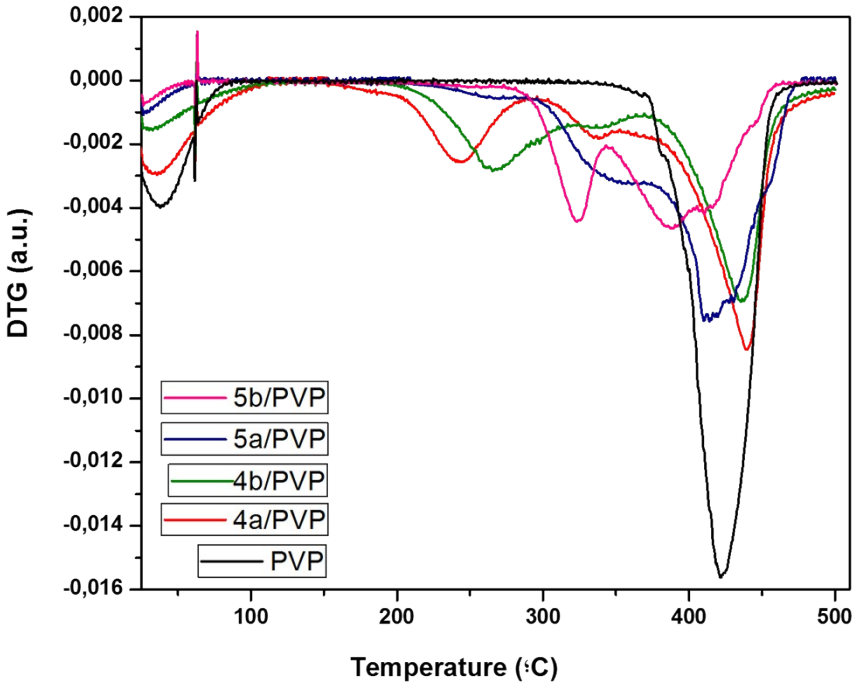

b)

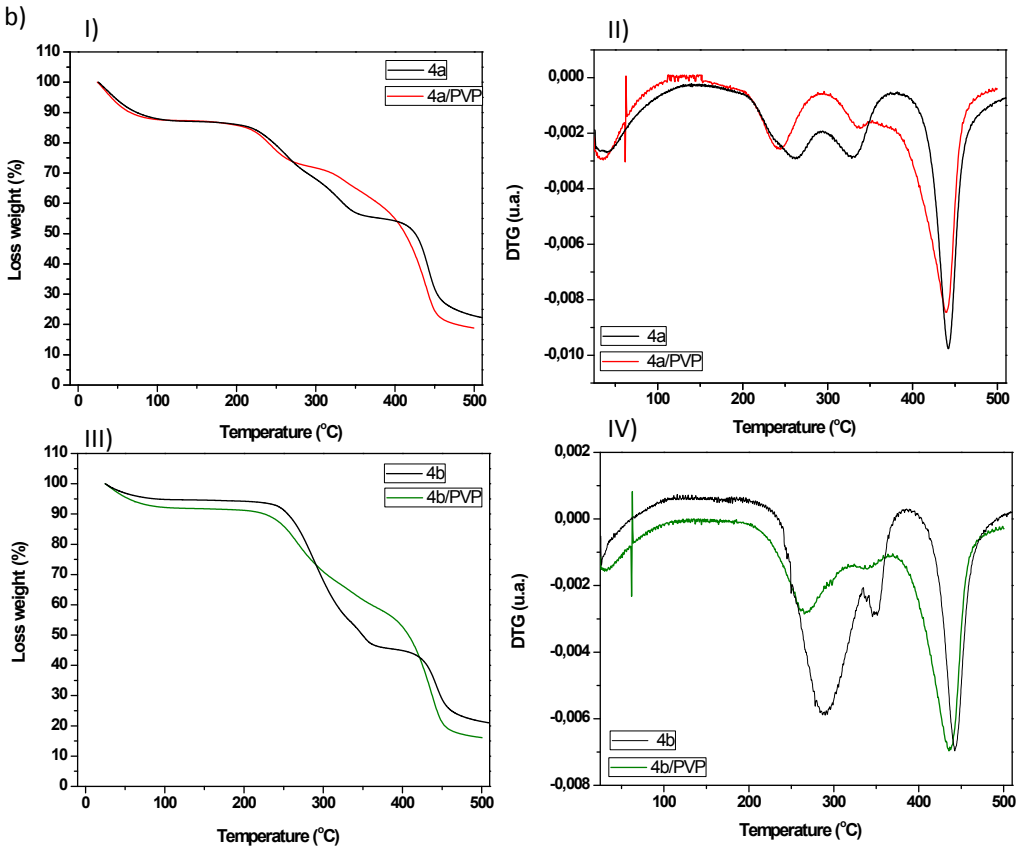

Figure S10. a) TGA (top) and DTA (bottom) obtained for the electrospun mats formed. b) TGA (right) and DTA (left) obtained for the electrospun mats and the related PILs for **4a** (top) and **4b** (bottom).

DSC results

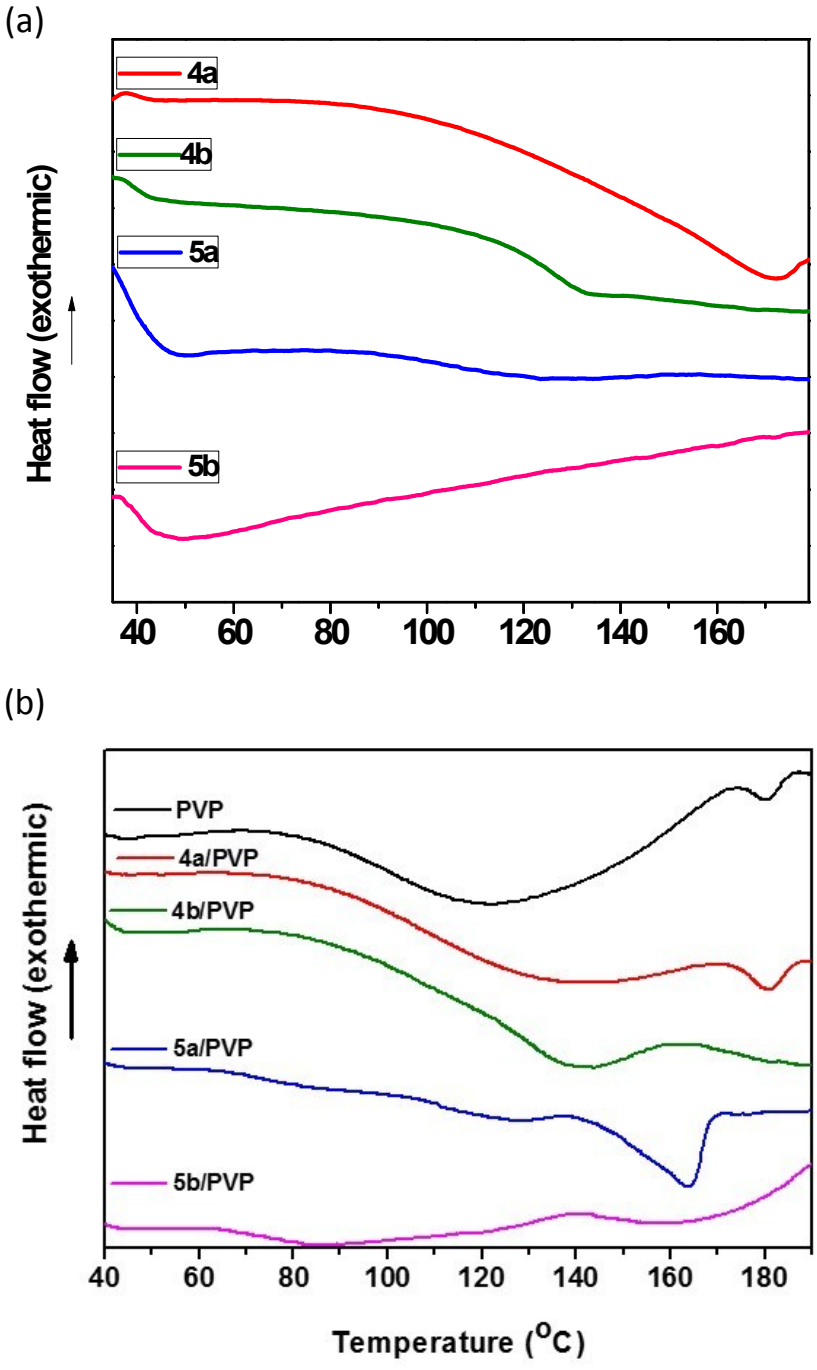

Figure S11. DSC for the PILs (a) and the different elesctrospun mats formed (b) (second heating cycle).

Oil/water separation process

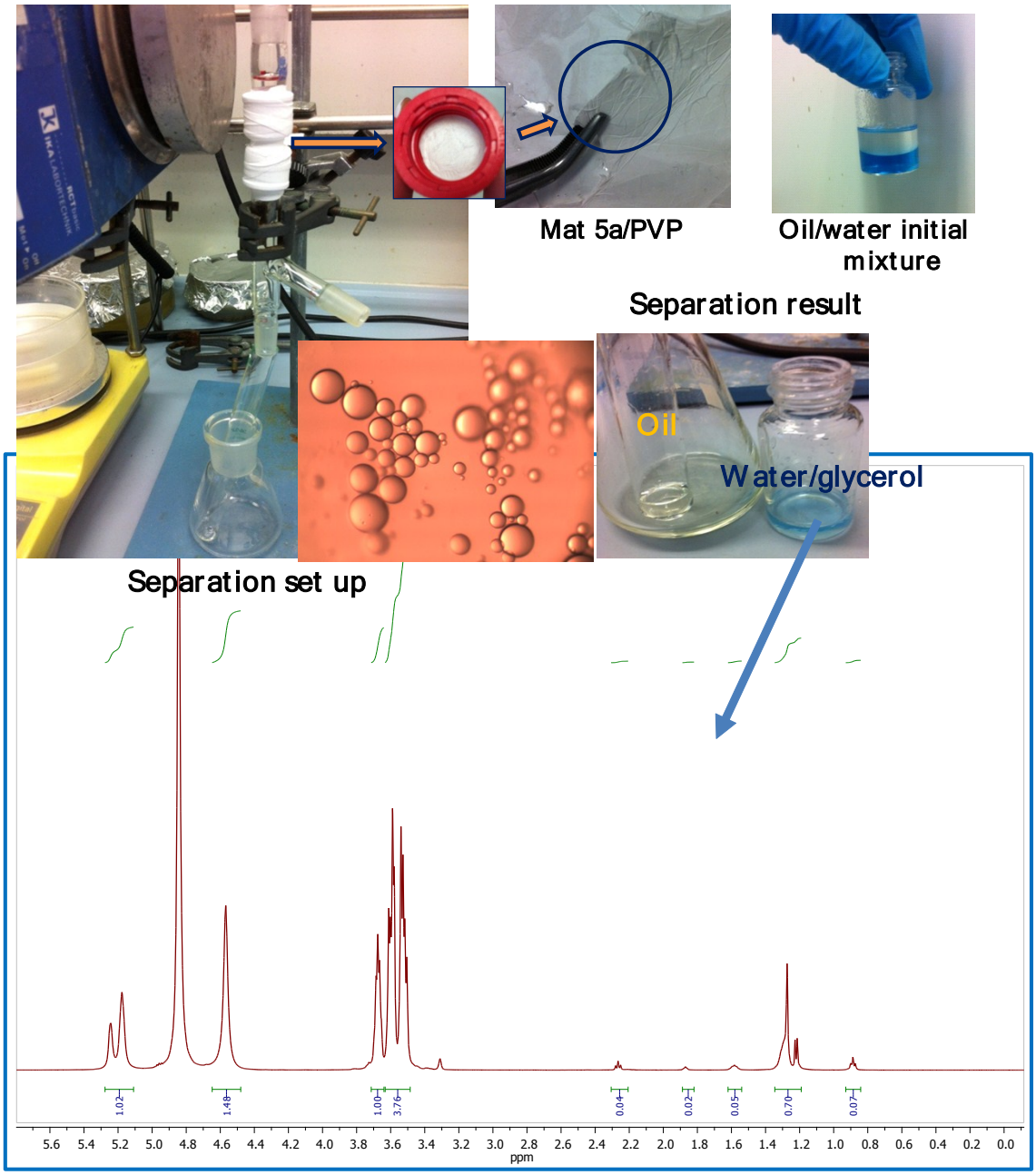

Figure S12. Separation of an oil / water emulsion and oil / glycerol/ water emulsion. IH (DMSO) of the water/glycerol Phase obtained after separation..

SEM and TEM images of AuNPs-films

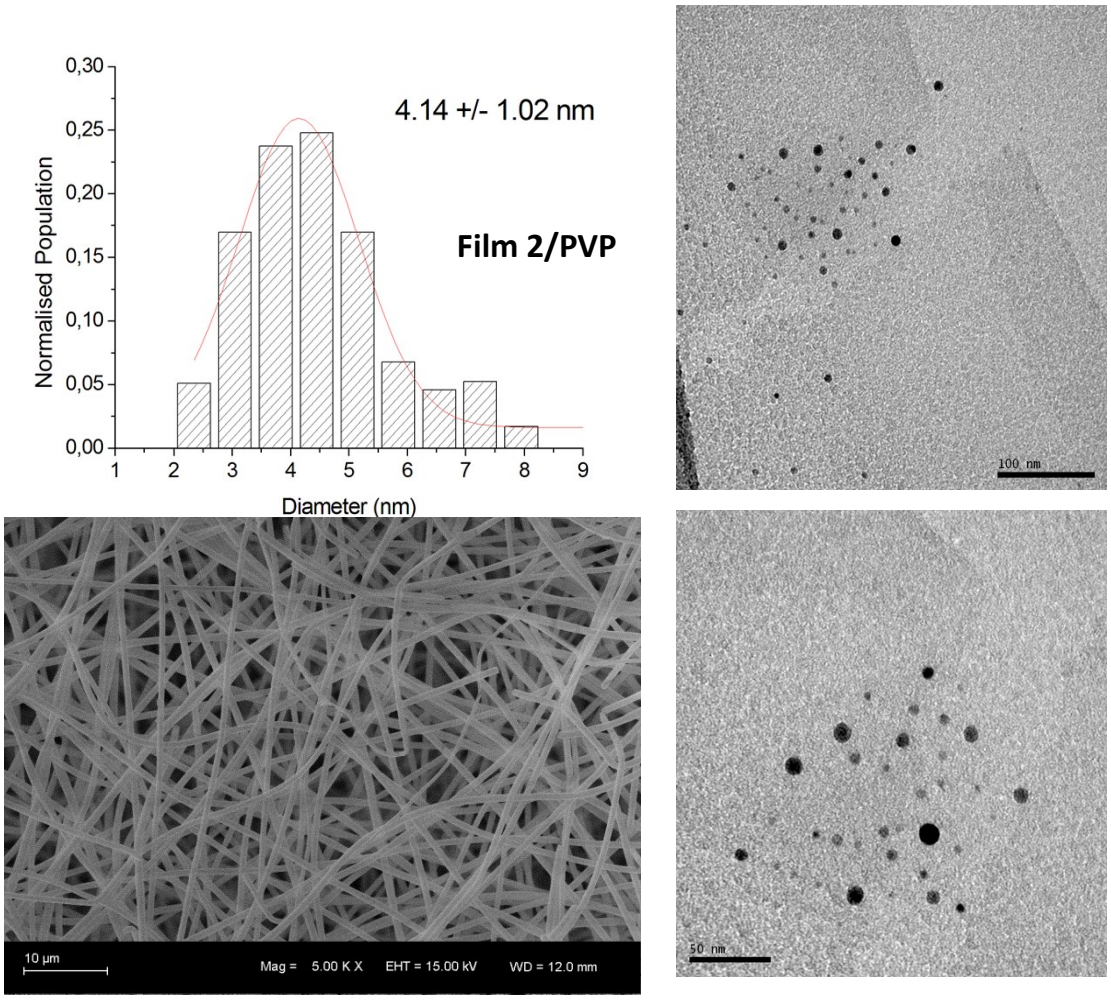

Spectrum	In stats.	C	N	O	F	S	Cl	Au	Total
3P53	Yes	51.24	2.93	2.76	0.14	0.62	5.27	37.04	100.00

Figure S13. SEM picture of the film **2/PVP**. TEM images of the AuNPs obtained after dispersing the film **AuNPs-2/PVP** in ethanol at 25 °C and the corresponding histogram and surface composition obtained by EDX analyses over the fibers after sputtering deposition.

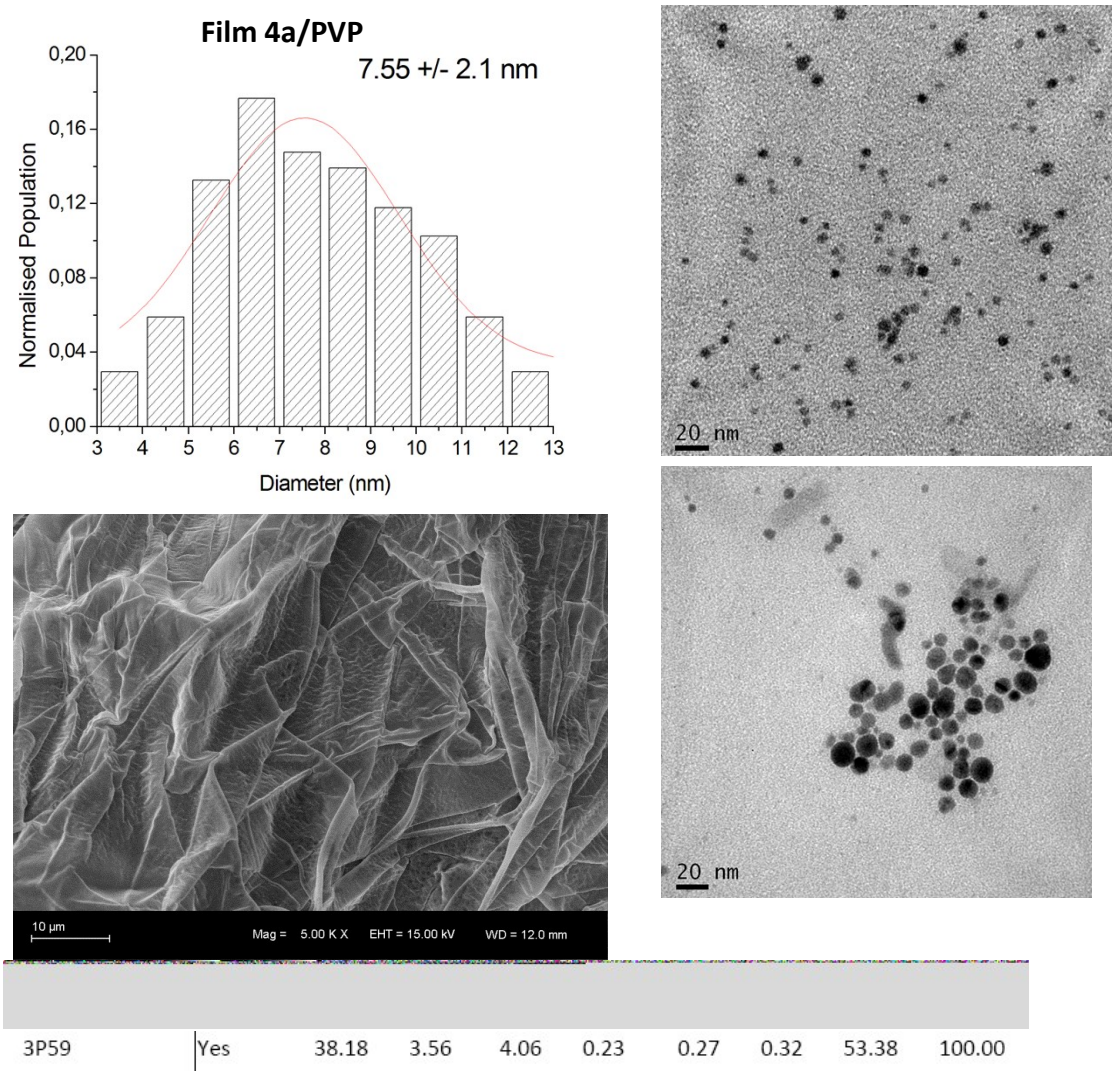

Figure S14. SEM picture of the film **4a/PVP**. TEM images of the AuNPs obtained after dispersing film **AuNPs-4a/PVP** in ethanol at 25 °C and the corresponding histogram and surface composition obtained by EDX analyses over the fibers after sputtering deposition.

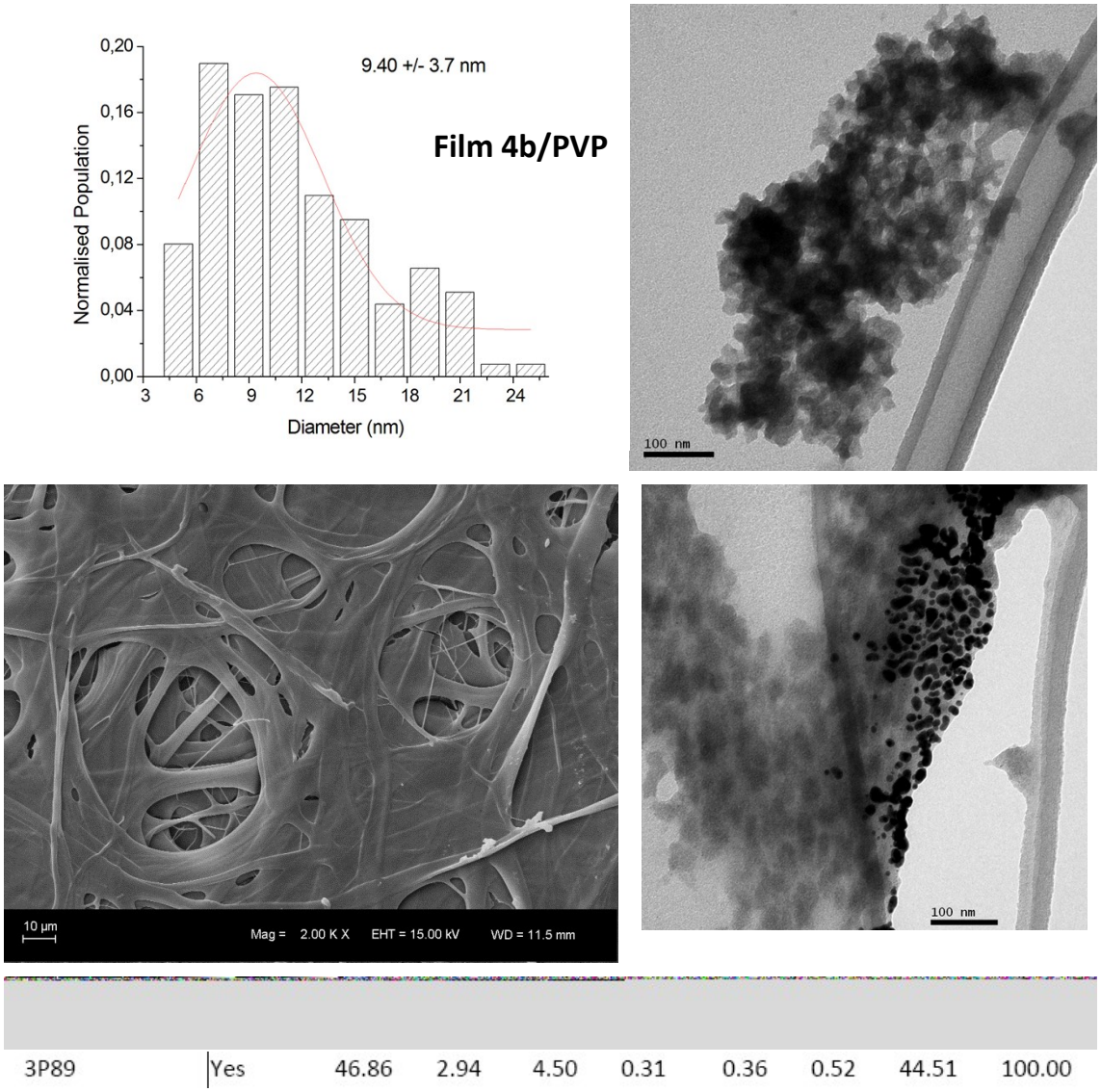

Figure S15. SEM picture of the film **4b/PVP**. TEM images of the AuNPs obtained after dispersing film **AuNPs-4b/PVP** in ethanol at 25 °C and the corresponding histogram and surface composition obtained by EDX analyses over the fibers after sputtering deposition.

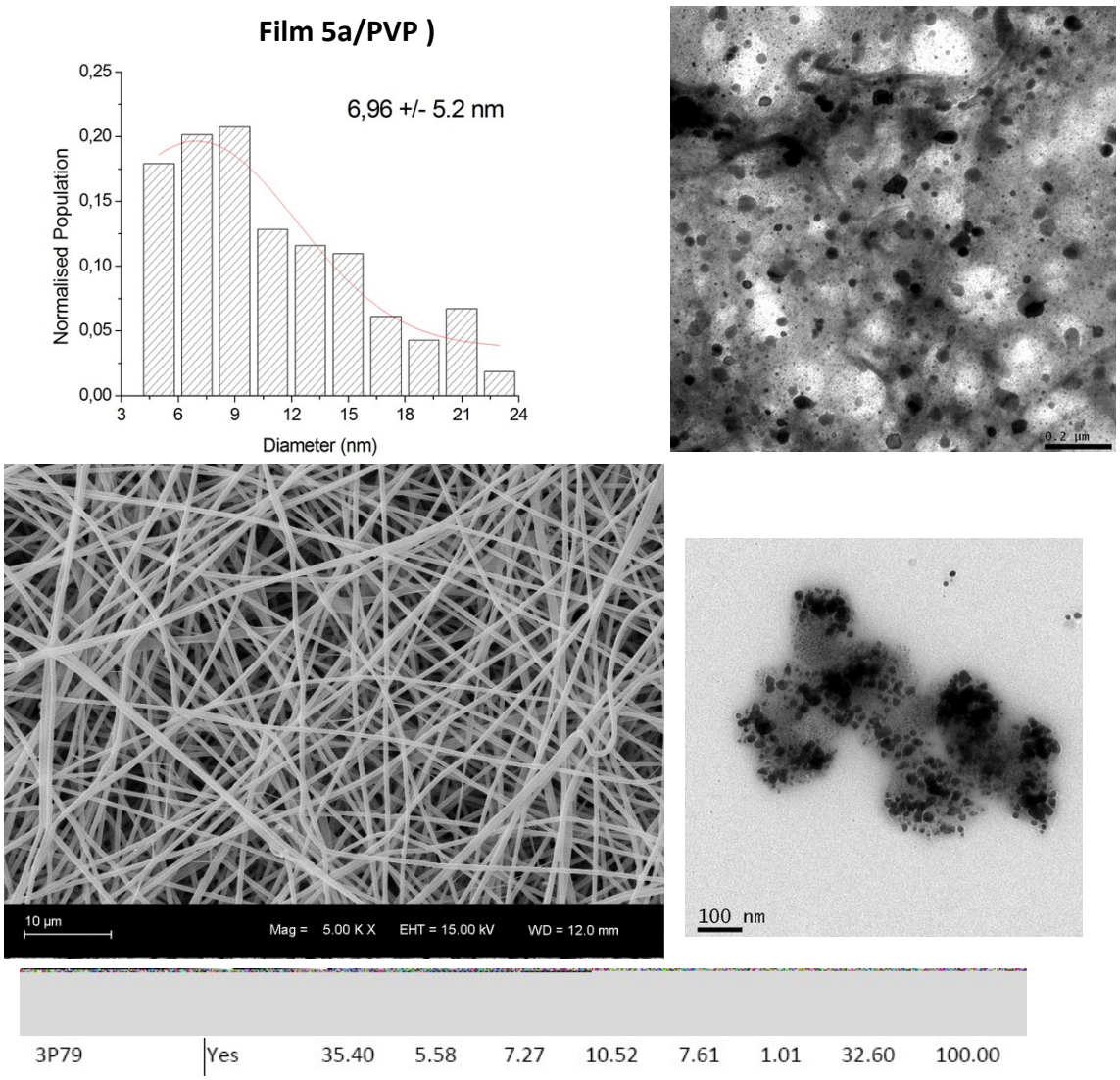

Figure S16. SEM picture of the film **5a/PVP**. TEM images of the AuNPs obtained after dispersing film **AuNPs-5a/PVP** in ethanol at 25 °C and the corresponding histogram and surface composition obtained by EDX analyses over the fibers after sputtering deposition.

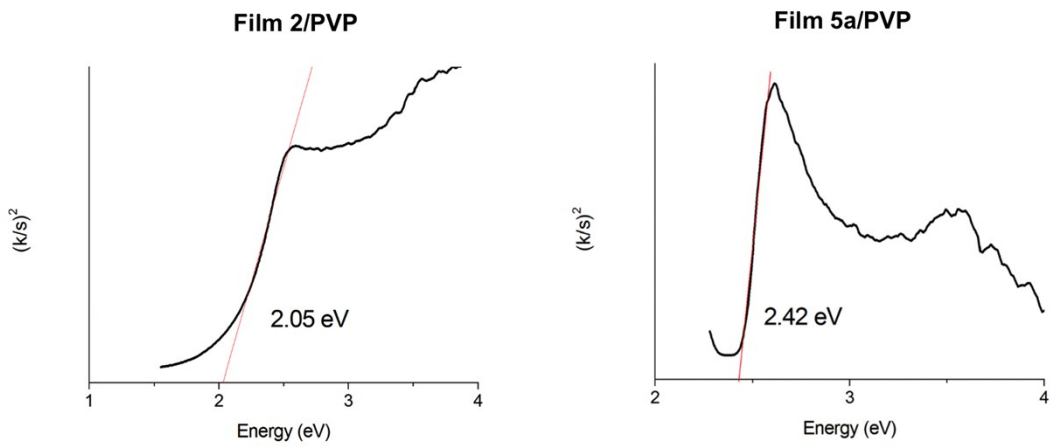

Figure S17. Diffuse UV-Vis analysis for the band gap determination of AuNPs supported onto nanostructured films.

Structural characterization of PILs: ^{1}H-NMR and IR spectra

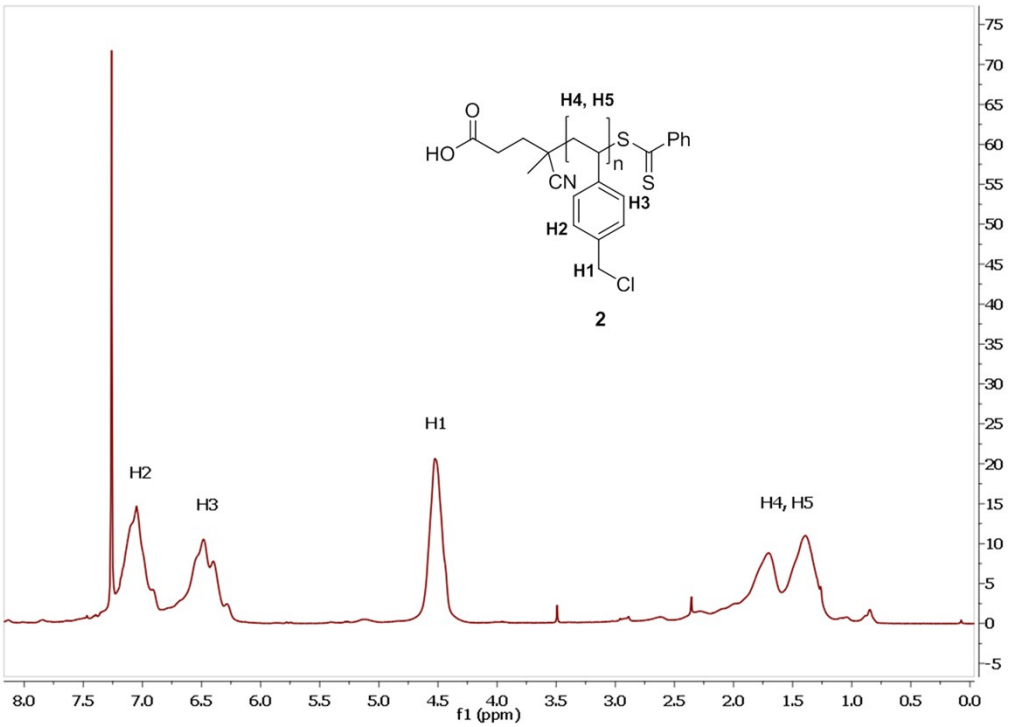

Figure S18. ^{1}H-NMR (500 MHz) with peak assignments for **2** ($CDCl_3$)

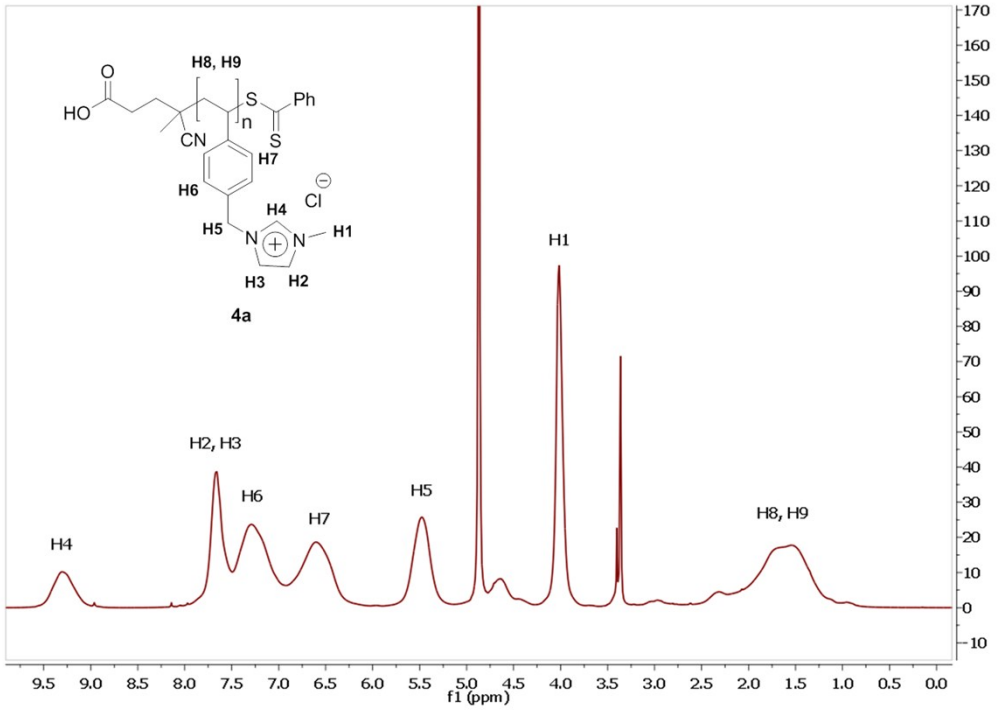

Figure S19. ^{1}H-NMR (500 MHz) with peak assignments for **PIL-4a** (MeOD)

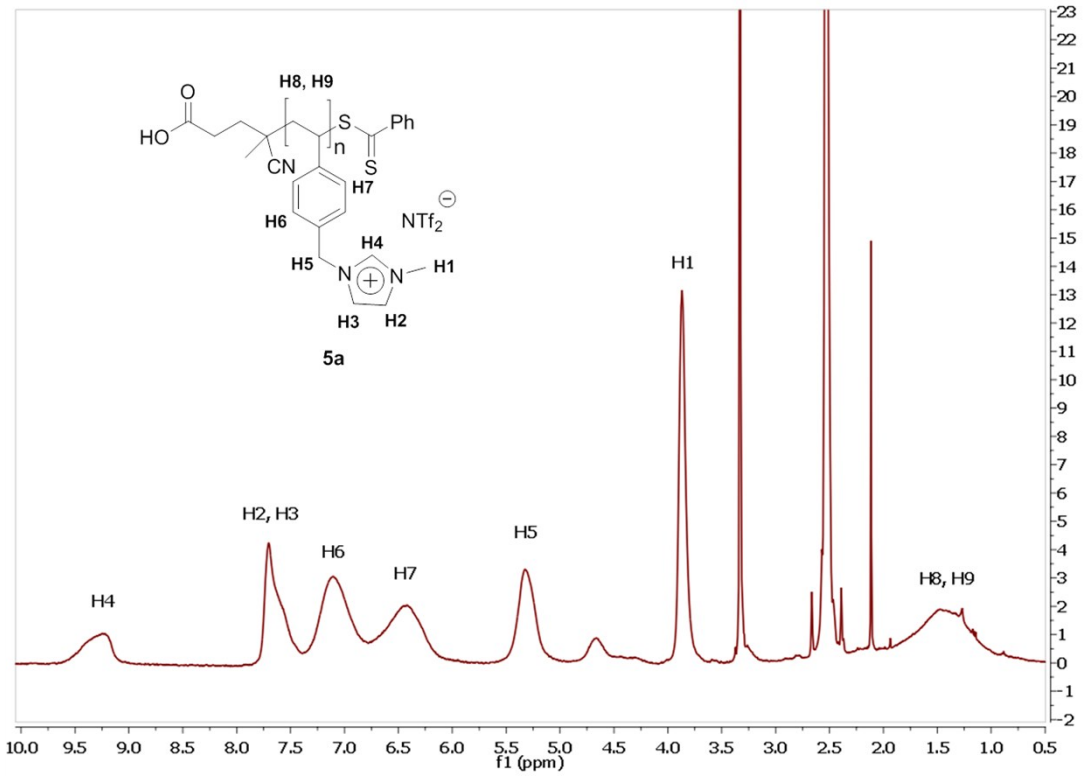

Figure S20. [1]H-NMR (500 MHz) with peak assignments for **PIL-5a** (DMSO-*d6*)

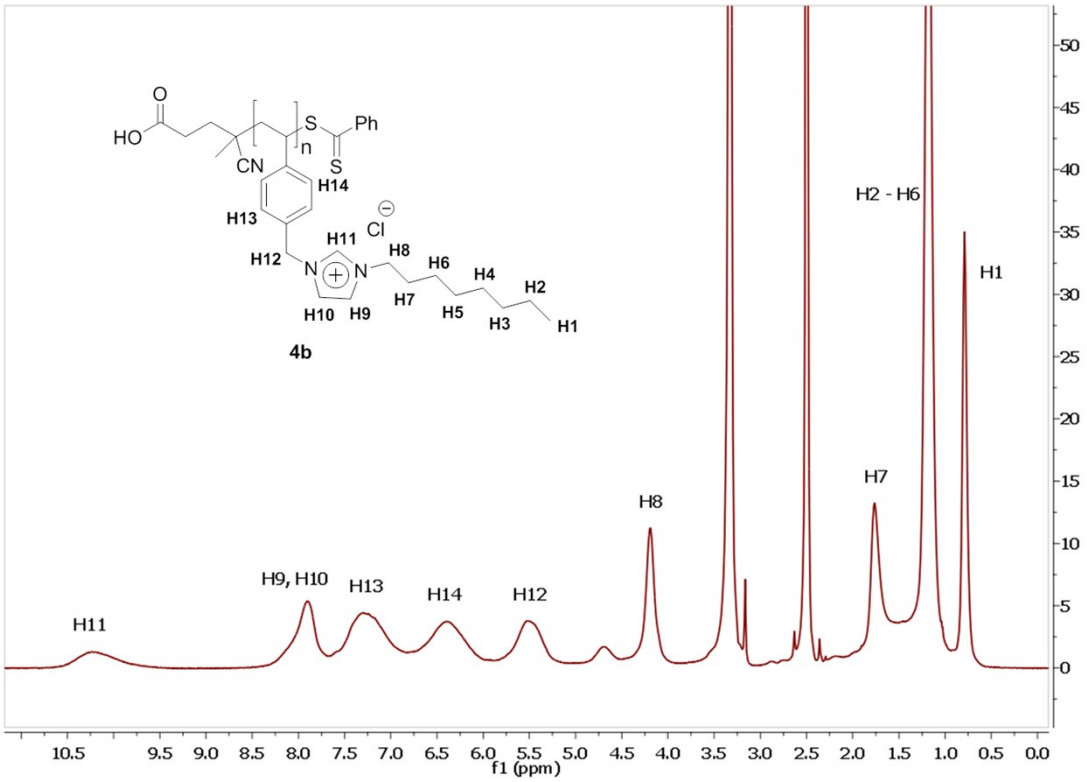

Figure S21. [1]H-NMR (500 MHz) with peak assignments for **PIL-4b** (DMSO-*d6*)

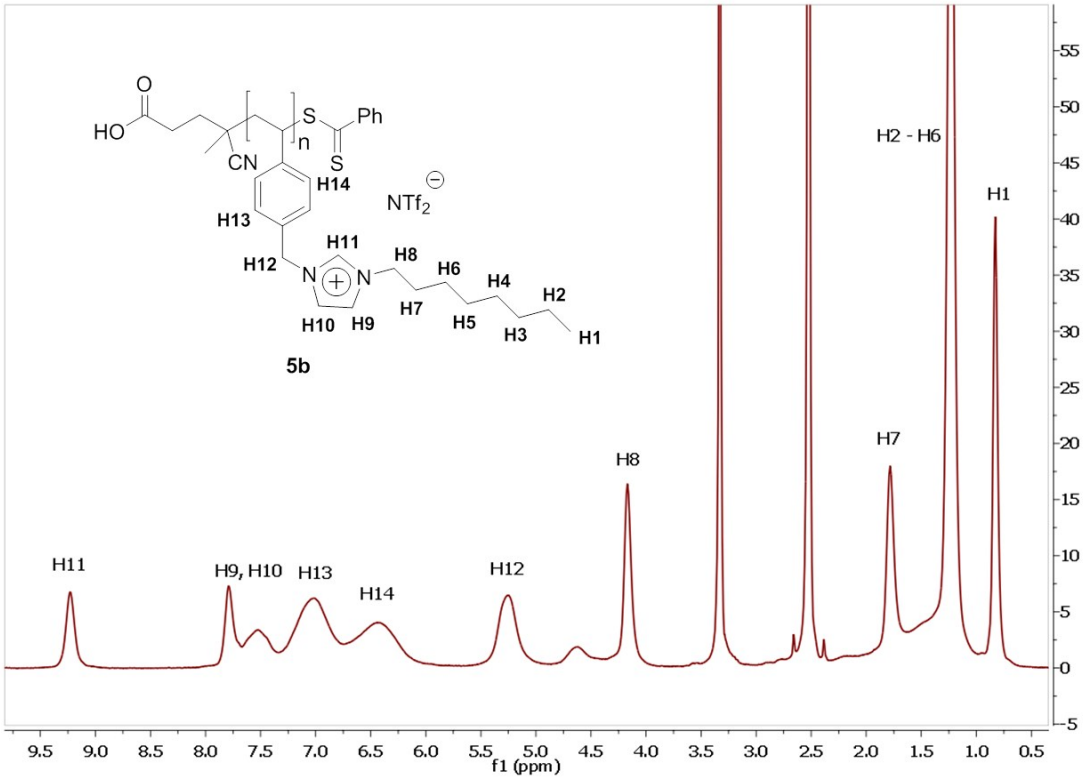

Figure S22. ^{1}H-NMR (500 MHz) with peak assignments for **PIL-5b** (DMSO-*d6*)

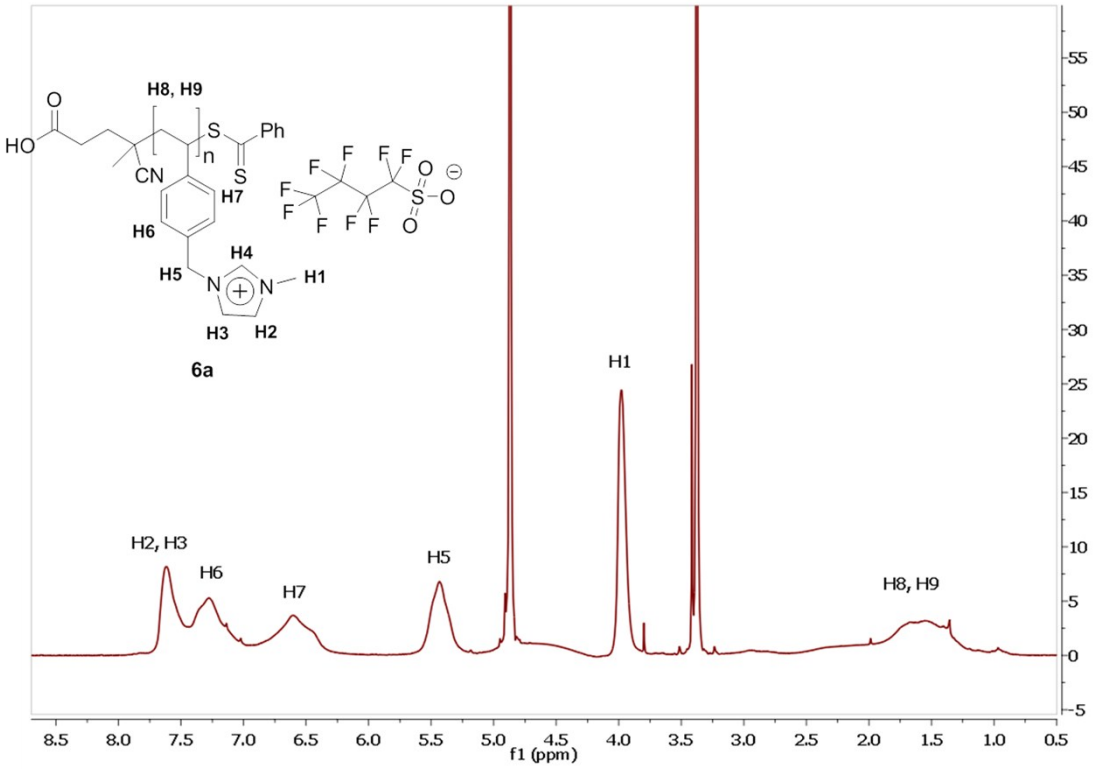

Figure S23. ^{1}H-NMR (500 MHz) with peak assignments for **PIL-6a** (MeOD)

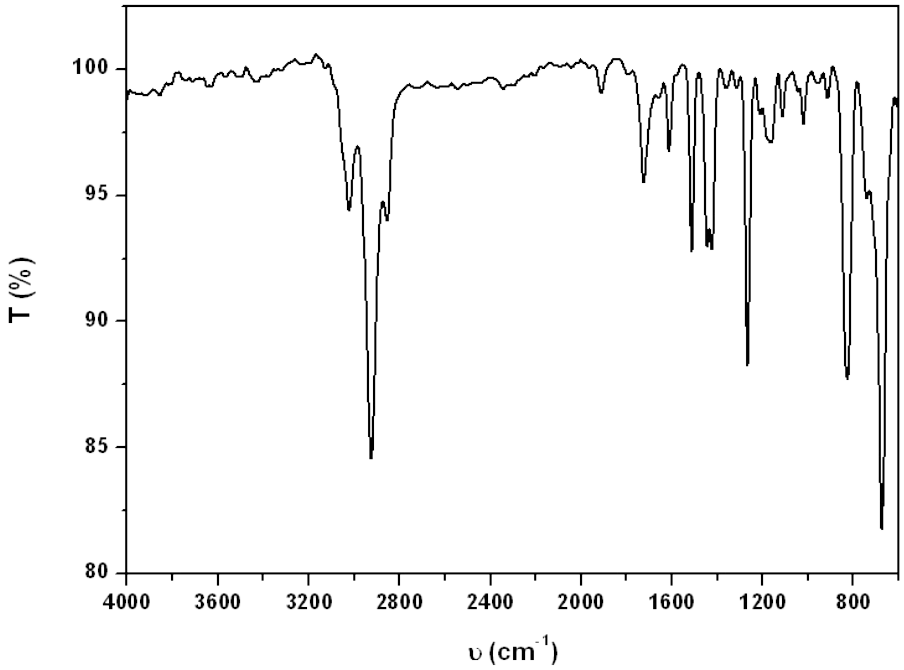

Figure S24. ATR-FT-IR for **2**

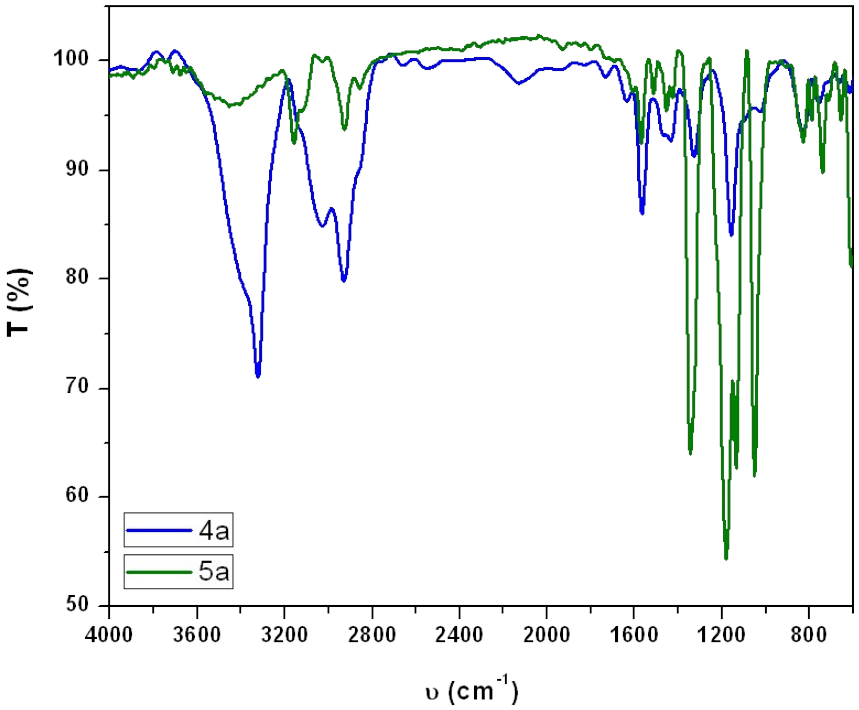

Figure S25. ATR-FT-IR for **PIL-4a** (*blue*) and **PIL-5a** (*green*)

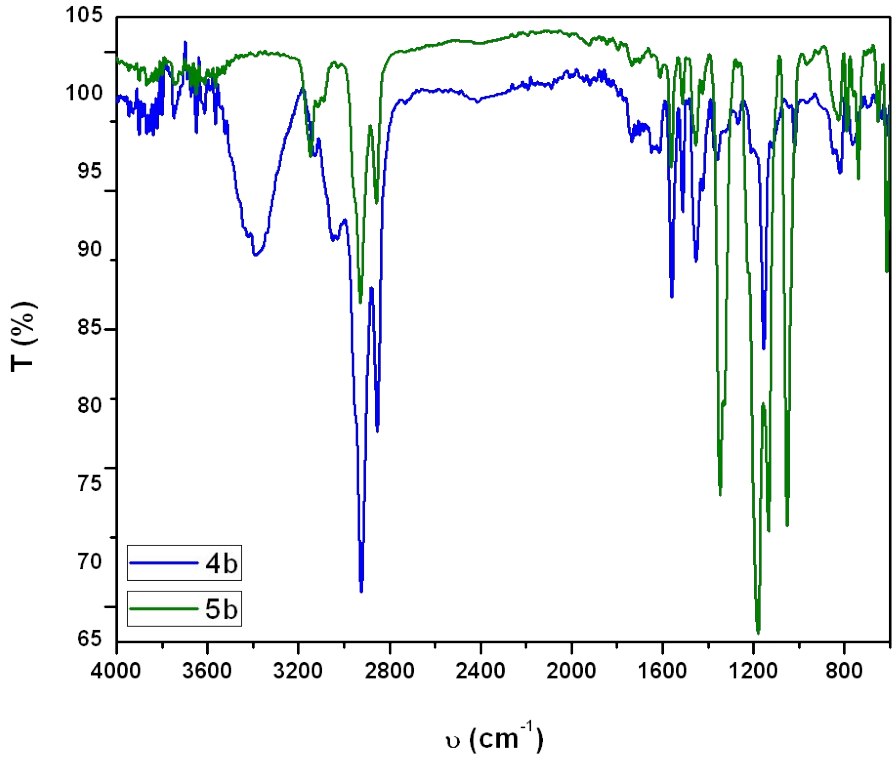

Figure S26. ATR-FT-IR for **PIL-4b** (*blue*) and **PIL-5b** (*green*)

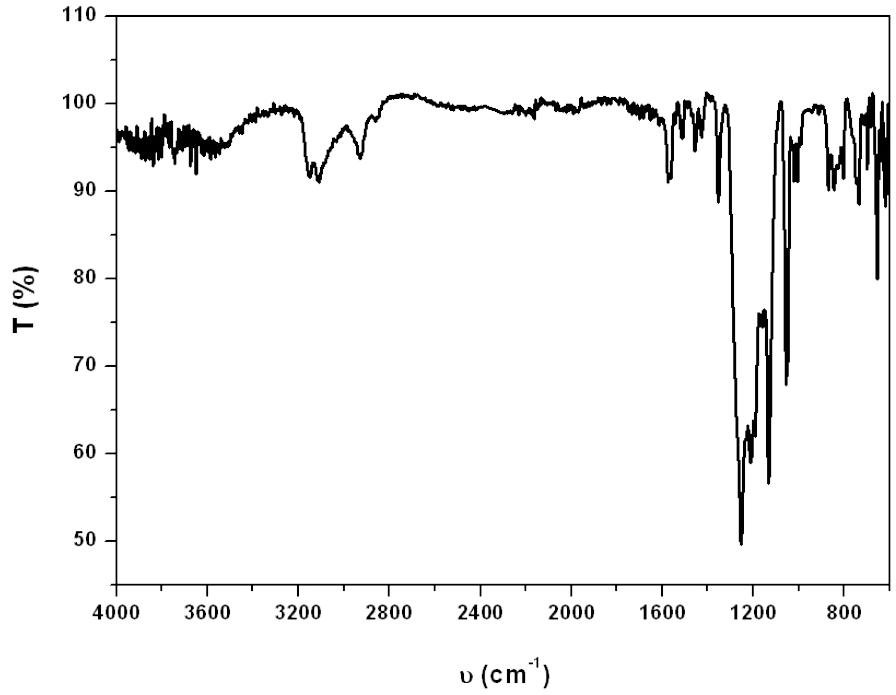

Figure S27. ATR-FT-IR for **PIL-6a**